Iodine capture with metal-functionalized polyacrylonitrile composite beads containing Ag^0, Bi^0, Cu^0, or Sn^0 particles

Saehwa Chong,[(a)] Brian J. Riley,[*,(a)] R. Matthew Asmussen,[(a)] Alessandra L. Fujii Yamagata,[(a)] José Marcial,[(a)] Sungsik Lee,[(b)] and Carolyne A. Burns[(a)]

[(a)] *Pacific Northwest National Laboratory, Richland, WA 99354*

[(b)] *X-Ray Science Division, Argonne National Laboratory, Lemont, IL 60439, USA*

Keywords: polyacrylonitrile; iodine capture; metal-polymer composites; silver; bismuth; copper; tin

Abstract

The capture of radioiodine from nuclear processes and the mitigation of environmental release is an important topic area of research. Some of the more commonly employed chemisorption-based iodine scavengers reported in the literature are based on metal-exchanged porous sorbents such as Ag-zeolites or metal-functionalized aerogels and xerogels. However, another option is to use zero-valent metals directly that have a known high affinity for iodine gas [i.e., $I_{2(g)}$]. In this study, fine metal particles of Ag^0, Bi^0, Cu^0, and Sn^0 were embedded in porous polyacrylonitrile (PAN) substrates at 75 mass% metal loadings within the form of ellipsoidal beads with maximum diameters of ~2–3 mm. These composite beads showed extremely high iodine loadings that are directly related to the metal particles loadings. The X-ray diffraction (XRD) analyses of Ag^0, Bi^0, Cu^0, and Sn^0 particles as well as metal-PAN composite beads reacted with iodine gas at 120±1°C showed phases of AgI, BiI_3, CuI, and SnI_4, respectively. For the Ag-PAN, Cu-PAN, and Sn-PAN beads, no other crystalline peaks were observed in XRD for unreacted metal or oxidized metals after 48-hour exposure to saturated $I_{2(g)}$ at 120±1°C, whereas unreacted metallic Bi^0 was observed within the Bi-PAN composites. However, after a 72-hour exposure at 120±1°C, both the Bi^0 particles and the Bi-PAN composites showed full conversion from Bi^0 to BiI_3 with XRD. Comparisons between mass uptake data and X-ray absorption spectroscopy were used to better understand the phase distribution of the Bi

[*] Corresponding author; brian.riley@pnnl.gov; (509)375-4651

phases present in the Bi-PAN+I composites. The iodine loadings (mg iodine per g sorbent, or q_e) for these materials were 1120 (Ag-Particle), 773 (Bi-Particle-72h), 1033 (Cu-Particle), 3000 (Sn-Particle), 753 (Ag-PAN), 1012 (Bi-PAN-72h), 1457 (Cu-PAN), and 1669 (Sn-PAN). It is possible that inexpensive sorbents such as these could be deployed to help limit or prevent release of radioiodine to the environment.

1 Introduction

Radioiodine is generated during fission of nuclear fuels and includes several radioisotopes including long-lived ^{129}I ($t_{1/2}$ = 1.57×10^7 years) and short-lived ^{131}I ($t_{1/2}$ = 8.02 days) that can be released during nuclear accidents or during reprocessing of used nuclear fuel. The release of radioiodine is a high-visibility environmental issue due to the detrimental effects on human health where it can lead to thyroid cancer.[1-5] Different solid sorbents including zeolites, aerogels, xerogels, chalcogels, porous organic polymers, and metal-organic frameworks have been studied for the capture of gaseous iodine[1,6-14] that utilize chemisorption, physisorption, or both as the method of capture. For metal-exchanged zeolite sorbents, the iodine loading capacities (q_e) generally range from 100 to 450 mg/g (mass of iodine per mass of starting sorbent).[14-23] For Ag-loaded aerogels, Ag-loaded xerogels, and Sn-based chalcogel sorbents, the q_e values are generally higher than metal-exchanged zeolites due to higher getter utilization and tend to range from 400 to >2000 mg/g.[24-30] This could be partially due to higher specific surfaces areas (m^2 g^{-1}) in the gel-based sorbents compared to the zeolites. In addition to these sorbents for gaseous radioiodine, other metal-based sorbents with porous scaffolds have been investigated such as Ag- or Bi-functionalized Ni-metal foams.[31] The metal foam approach might provide a method for combining the active metal sites with an active porous metal support, depending on the metal used for the foam support. For radioiodine chemisorption, a few different getter metals have been identified as having both high iodine affinity and low metal-iodide leach rates that include Ag, Bi, Cu, and Pb,[32-35] which could help solve both the iodine capture need and the long-term stability need for disposal of radioiodine in a geological repository.

In this study, the iodine loading capacities of as-received Ag^0, Bi^0, Cu^0, and Sn^0 metal particles were compared with hybrid sorbents containing these same metals embedded in polyacrylonitrile (PAN)-

based composite beads. These sorbents show high iodine loading capacities (q_e = 474–3000 mg per gram of initial sorbent) and their appearances, micro/macrostructures, and chemistries were investigated with optical microscopy, pycnometry, X-ray diffraction (XRD), scanning electron microscopy (SEM), and energy dispersive X-ray spectroscopy (EDS). X-ray absorption hear-edge structure (XANES) analyses, including Bi L_3 and I L_3 edges, were also conducted on the Bi-containing materials. This work was based off our previous study evaluating pure metal wires without the porous polymer scaffold[34] and the 75 mass% loadings used were based on previous work on embedding active particle or powdered sorbents into PAN composites.[30,36-42] Due to kinetics limitations of iodine vapors reacting through thick (0.5 mm) wires from a separate study,[34] small particles were selected for use in the current study as the active metal sites.

2 Experimental

2.1 Synthesis of metal containing PAN composites

Scheme 1 provides an overview of the process used to create the metal-PAN composites. Fine metal particles of Ag^0 (635 mesh, 99.9%), Bi^0 (325 mesh, 99.5%), Cu^0 (10 μm, 99.9%), and Sn^0 (325 mesh, 99.8%) acquired from Alfa Aesar were used as received. Information on the precursors and sample synthesis details are provided in Table 1. For the synthesis of each PAN composite, ~0.2 g of PAN fibers (×100, 3.3 dtex, 60 mm; Dralon GmbH, Dormagen, Germany) were separately dissolved in 3 mL of dimethyl sulfoxide (DMSO; ≥99.9%, Sigma Aldrich) within a 20-mL Pyrex beaker covered with Parafilm (Scheme 1a, Step-1). After the PAN fibers were completely dissolved (~15 min), ~0.6 g of metal particles were slowly added to the DMSO-PAN mixture (75 mass% active metal in the total solids), and the mixture was stirred over a time of ~5 min until it was homogenously suspended in the mixture (Scheme 1b, Step-2). To prevent particle settling, the mixture was stirred continuously just up to the point of the next step. This mixture of metal, PAN, and DMSO was slowly poured in batches into 5 mL pipette tip positioned at ~5 cm above a stirring 150-mL deionized water (DIW, >18.2 MΩ-cm) bath at 1–7 °C, where the cooler temperatures were achieved by placing this DIW dish inside a separate ice water bath (Scheme 1c, Step-3). The droplets were gravity assisted into the DIW water dish and formed into metal-PAN composite beads

with “oblate spheroidal external surfaces” as described in our previous study using this same process with different active getters.[37] After stirring in the DIW water bath for 10 min, the beads were transferred to a separate dish with fresh DIW two separate times for a total of ~400 mL of DIW exposure over the course of 30 minutes to aid in DMSO removal of bead interiors through passive diffusion. After these DIW exchanges, the beads were removed from the third dish, blotted dry with a paper towel, transferred to separate glass scintillation vials for each different bead type, and dried in a vacuum desiccator at room temperature over the course of a 2–3 weeks (Scheme 1d, Step-4). The same synthesis method was used for all four metal-PAN composites, and each metal-PAN composite contained 75 mass% of metal (on a solids basis). For naming the samples, Ag^0-, Bi^0-, Cu^0-, and Sn^0-based metal-PAN composite beads were denoted as Ag-PAN, Bi-PAN, Cu-PAN, and Sn-PAN, respectively.

2.2 Gaseous iodine loading into metal-PAN composites and particles

Iodine loadings for both the metal-PAN composites and metal particles were performed at 120±1 °C to estimate the loading capacity of gaseous iodine using a high-precision oven (Thermo Scientific Lindberg Blue M). For these experiments, 0.01–0.04 g of each sorbent sample (m_s) was placed into separate tared 4 mL glass vials (Qorpak GLC-00980). The masses of metal particles (m_m) added equated to ~75 mass% of the total solids masses in the composite beads so the total getter masses for all samples was similar (assuming no reaction from the PAN in the metal-PAN composites). All the open vials containing metal-PAN composites and metal particles were placed into 1 L perfluoroalkoxy (PFA) jar (Savillex, Eden Prairie, MN). A glass vial containing solid iodine pieces (99.99%, Sigma Aldrich) and a 4 mL blank vial were also placed into the PFA jar. Additionally, Ag-faujasite (IONEX Ag-400) was added as a standard to each iodine-loading run.

The mass of solid iodine was equal to 1.5× the stoichiometric amount needed for full conversion of Ag^0, Bi^0, Cu^0, Sn^0 into AgI, BiI_3, CuI, and SnI_4, respectively; the blank vial was added to check iodine adsorption on the vial (for background corrections). The PFA jar was tightly sealed and placed into the oven at 120±1 °C for 48 h, and then the vials were removed from the container and placed in a separate

oven (Fisher Scientific Isotemp 3511FSQ) at ~100±8 °C for 1 h to remove weakly physisorbed iodine. For naming the samples, iodine-loaded Ag-PAN, Bi-PAN, Cu-PAN, and Sn-PAN metal-PAN composite beads were given a "+I" suffix (e.g., Ag-PAN+I). For particle samples without PAN, similar notations were used (e.g., Ag-Particle+I). For Bi-PAN and Bi^0 particles, additional experiments were done at 24 h and 72 h with a similar experimental setup and the time was added as a suffix to the sample names [e.g., Bi-PAN+I(24h)]. A total of four separate iodine loading runs were run including (1) the 48-h run with Ag-Particle, Ag-PAN, Bi-Particle, Bi-PAN, Cu-Particle, and Cu-PAN; (2) the 48-h run with Sn-Particle and Sn-PAN; (3) the 24-hr run with Bi-Particle and Bi-PAN, and (4) the 72-hr run with Bi-particle and Bi-PAN.

Using Equations (1), (2), and (3), the gravimetric iodine capacities of the pure metal particles and the metal-PAN composites were calculated where m_s was the starting mass of the sample, m_{s+I} is the final mass following iodine capture, m_I was the mass of iodine captured by the sample based on mass changes, $m\%_I$ was the mass% of iodine in the final sample, and iodine loading (Q_e) is denoted as m_I/m_s, which is the mass of iodine captured per starting mass of the sorbent (in g/g). Often times another term is used in the literature called q_e, which utilizes the milligrams of iodine per gram of sorbent mass (mg/g) or $1000 \cdot m_I/m_s$, which is shown in Equation (4).

$$m_I = m_{s+I} - m_s \tag{1}$$

$$m\%_I = 100 \cdot \left({}^{m_I}/_{m_{s+I}}\right) \tag{2}$$

$$Q_e = {}^{m_I}/_{m_s} \text{ (g/g)} \tag{3}$$

$$q_e = 1000 \cdot {}^{m_I}/_{m_s} \text{ (mg/g)} \tag{4}$$

Based on the data derived from these equations, additional calculations were made, as described below. The first calculation was the maximum iodine mass possible ($m_{I,max}$) based on initial sorbent mass

(m_s) shown in Equation (5), which is based solely on metal-iodine chemisorption to fully react metals into the expected metal-iodide complexes (MI_x; i.e., AgI, BiI_3, CuI, and SnI_4 for Ag^0, Bi^0, Cu^0, and Sn^0, respectively, assuming no reaction with the PAN matrix) where mf_{ML} is the mass fraction of metal loading in the sorbent (i.e., 1.00 for metal particles and 0.75 for metal-PAN composites), x_I is the molecular weight of iodine, x_m is the molecular weight of the base metal in the sorbent, and M_I is the moles of iodine in the reacted metal-iodide compound (MI_x; e.g., $M_I = 3$ for BiI_3). Additionally, the maximum possible Q_e values ($Q_{e,max}$) can be determined using Equation (6) utilizing the initial sample mass (m_s) and the $m_{I,max}$ value calculated from Equation (5). Alternatively, these values were also calculated in terms of mg/g loadings using the $q_{e,max}$ notation shown in Equation (7).

$$m_{\mathrm{I,max}} = \frac{m_{\mathrm{s}} \cdot mf_{\mathrm{ML}} \cdot x_{\mathrm{I}} \cdot M_{\mathrm{I}}}{x_{\mathrm{m}}} \tag{5}$$

$$Q_{\mathrm{e,max}}\ (\mathrm{g/g}) = {}^{m_{\mathrm{I,max}}}/_{m_{\mathrm{s}}} \tag{6}$$

$$q_{\mathrm{e,max}}\ (m\mathrm{g/g}) = 1000 \cdot Q_{\mathrm{e,max}} \tag{7}$$

The total mass of metal-iodide in the reacted sorbent ($m_{m\text{-}I}$) was calculated with Equation (8) based on the total mass gain and all gained mass was assumed as metal converted to a metal iodide (MI_x), where $x_{m\text{-}I}$ is the molecular weight of the metal-iodide compound, and the other variables were previously defined. Based on the data from the above calculations, the residual (unreacted) metal present in the sorbent ($m_{m,r}$) can be calculated with Equation (9) where the variables were previously defined. Then, the conversion% (C%m) based on mass data alone can be calculated using Equation (10) with the m_I and $m_{I,max}$ values or $m_{m,r}$ and m_m and values. These calculations assume all mass uptake was iodine capture and that no water (or other chemical, e.g., residual DMSO) adsorption/desorption occurred from the metal-PAN composites or the metal particles during the iodine-loading experiments.

$$m_{\text{m-I}} = \frac{m_{\text{I}} \cdot x_{\text{m-I}}}{x_{\text{I}} \cdot M_{\text{I}}} \tag{8}$$

$$m_{\text{m,r}} = m_{\text{s+I}} - m_{\text{PAN}} - m_{\text{m-I}} \tag{9}$$

$$C\%\text{m} = 100 \cdot {m_{\text{I}}}/{m_{\text{I,max}}} = 100 \cdot {\left(m_{\text{m}} - m_{\text{m,r}}\right)}/{m_{\text{m}}} \tag{10}$$

Finally, the mass fraction values of the iodine-loaded sorbent constituents can then be calculated to further compare some of the datasets using Equation (11) for PAN (mf_{PAN}), Equation (12) for the residual metal ($mf_{\text{m,r}}$), and Equation (13) for the MI_x loading ($mf_{\text{m-I}}$). Additional calculations are provided in the Supporting Information. The values of $mf_{\text{NP,m,r}}$ and $mf_{\text{NP,m-I}}$ calculated using Equation (14) and Equation (15) are mass fractions from renormalizing after removing the m_{PAN} ("NP" subscript denotes "no PAN") from the calculations in Equation (12) and Equation (13), respectively, so they are just comparing changes in $m_{\text{m,r}}$ and $m_{\text{m-I}}$.

$$mf_{\text{PAN}} = {m_{\text{PAN}}}/{(m_{\text{s+I}})} \tag{11}$$

$$mf_{\text{m,r}} = {m_{\text{m,r}}}/{(m_{\text{s+I}})} \tag{12}$$

$$mf_{\text{m-I}} = {m_{\text{m-I}}}/{(m_{\text{s+I}})} \tag{13}$$

$$mf_{\text{NP,m,r}} = {m_{\text{m,r}}}/{(m_{\text{s+I}} - m_{\text{PAN}})} \tag{14}$$

$$mf_{\text{NP,m-I}} = {m_{\text{m-I}}}/{(m_{\text{s+I}} - m_{\text{PAN}})} \tag{15}$$

2.3 Iodine capture in the aqueous medium

Iodide (I^-) removal was evaluated for the Ag-PAN, Bi-PAN, and Cu-PAN composites. Here, each of the composites were added to separate 15 mL centrifuge vials, and then 10 mL of a caustic scrubber simulant was added (Table S1, Supporting Information). The samples were mixed with a rotary mixer (Model AD3740-12RA10 Phipps & Bird, Inc.) for 24 h with 1 mL aliquots collected at 0 h, 1 h, 4 h, and 24 h. The amounts of media added corresponds to an equimolar of Ag/Bi/Cu fraction and I^- concentration. The aliquots were stabilized with 0.5 vol% of UniSolv Neutralizing and Stabilizing Reagent (UNS-2B, Inorganic Ventures) and submitted for inductively coupled plasma mass spectroscopy (ICP-MS) for ^{127}I and ion chromatography (IC) for the other anions. For ICP-MS, iodine was measured quantitatively for mass 127 using a Thermo Scientific X-Series quadrupole instrument with an Elemental Scientific SC4 DX FAST auto-sampler interface. For IC, samples were quantitatively measured using a Dionex Reagent Free IC System (RFICS) 2000 with an AS-1 auto-sampler interface or a Dionex RFICS 5000 with an AS-AP auto-sampler interface.

2.4 Characterizations

2.4.1 Photography and optical microscopy

Photographs were captured of the samples using a Rebel T7 digital camera (Canon U.S.A., Inc., Huntington, NY) on a tripod using the Canon EOS Utility software (v3.15.20). Optical micrographs were taken of the samples using a ProgRes SpeedXT^{core} 5 (Jenoptik, Jena, Germany) connected to a Leica $MZ12_5$ stereo microscope. Pictures were taken of a ruler at the same magnifications for each image so that scalebars could be added later in Adobe Photoshop (v23.5.1).

2.4.2 Density (pycnometry)

Densities of metal-PAN beads were calculated using measured volumes by a helium pycnometer (Micromeritics AccuPyc II 1340). The accuracy of volume measurement was checked with the standard sphere from Micromeritics before the volume measurement. The sample cup of 1 cm^3 was filled with metal-PAN beads and inserted into the pycnometer and 10 volume measurements were performed for each

sample. Using AccPyc II software, the densities were calculated with the average volumes and inputted sample masses.

2.4.3 X-ray diffraction

For XRD analyses, crushed metal-PAN composites and metal particles were placed on zero-background quartz holders (MTI corporation, Richmond, CA) and scanned with a Bruker D8 Advance X-ray diffractometer (Bruker AXS Inc., Madison, WI) with a Cu source and a LynxEye position-sensitive detector or scintillator detector, and the scan parameters were 10–70° 2θ with a step of 0.02° and 1–4 s dwell times per step. For the phase identification and quantification, Bruker AXS DIFFRAC^{plus} EVA (v4.1) and TOPAS (v5) software programs were used, respectively, using crystallographic information files from the Inorganic Crystal Structure Database for refinements (v4.8.0, build 20220419-1910; FIZ Karlsruhe GmbH).

2.4.4 Scanning electron microscopy and energy dispersive X-ray spectroscopy

The SEM-EDS analyses were performed with a JSM-7001F field-emission gun microscope (JEOL USA, Inc.; Peabody, MA) on metal particles and metal-PAN composites cut into halves and adhered to aluminum stubs with carbon tape. The EDS analyses were performed with a Bruker xFlash 6|60 detector (Bruker AXS Inc., Madison, WI). Samples were not coated and were analyzed in low-vacuum mode (30 Pa) to prevent charging artifacts.

2.4.5 Particle size distribution

Particle size distributions (PSDs) were measured on the as-received metal particles using a Mastersizer 2000 (Malvern Instruments, Inc., Southborough, MA) with a HydroS wet dispersion accessory with a measurement range of 0.02–600 μm. Measurements were made before, during, and after sonication, allowing determination of the influence of sonication on the distribution of particle sizes within the sample.

2.4.6 Metal-PAN composite measurements

The metal-PAN composites were measured with the measurement tool in Adobe Photoshop (v23.5.1) by taking pictures of several beads using a MZ12$_5$ microscope (Leica Microsystems, Deerfield,

IL) along with pictures at the same magnification with a NIST Micro-Ruler (Geller MicroÅnalytical Laboratory, Inc., Topsfield, MA). Measurements were made on the smallest and largest dimensions of sitting beads, which excluded the third dimension, that was likely the smallest of the three diameters. Values were averaged and standard deviations (±1σ) were calculated.

2.4.7 X-ray absorption near-edge structure

XANES analyses were performed near the Bi L_3-edge (13.419 keV) and the I L_3-edge (4.557 keV) at the 12-BM-B beamline of the Advanced Photon Source (APS) at Argonne National Laboratory using a Si(111) monochromator. The data were collected in transmission and fluorescence modes simultaneously, however only data captured in fluorescence mode were utilized for this study. For preparing samples, approximately 5–10 mg of sample powders were used with no binder while 2–3 mg standards were separately mixed with ~ 2–3 mg of carbowax polyethylene glycol (PEG) molecular weight 8000 binder (Fisher, >95%) and pressed into 7-mm diameter pellets at 70 MPa using a uniaxial press then cut to fit the sample holders.

Linear combination fittings of Bi L_3-edge XANES spectra were performed to estimate the Bi speciation in the samples as well as the redox ratio of Bi^{3+}/Bi^0. This approach assumed that each sample was a linear combination of measured spectra (s_i) from Bi^0 (Bi metal, Thermo Scientific 99.5%) and Bi^{3+} species [i.e., Bi_2O_3 (Alfa Aesar, 99.975%), BiOI (Alfa Aesar, >98%), and/or BiI_3 (Alfa Aesar, 99.999%) after iodine sorption] with these four species summing to 1, shown in Equation (16), where r_i is the mole fraction of species "i" (denoted in brackets) within the sample. The concentrations for the four species were fit to data using a least-squares approach.

$$\sum_{i=1}^{n} r_i s_i = r_1[Bi^0] + r_2[Bi_2O_3] + r_3[BiOI] + r_4[BiI_3] = 1 \quad (16)$$

The I L_3-edge XANES analyses were performed utilizing beamline 12-BM-B at APS operated in fluorescence mode using a Si(111) monochromator and calibrated using AgI powder (Alfa Aesar, Premion,

99.999%). The step size for I L_3-edge measurements were 5.0 eV (for the energy range of 4.410–4.547 keV), 0.4 eV (for 4.547–4.577 keV), and 0.05 $Å^{-1}$ (for 4.577–4.800 keV). These data were not used for phase quantifications, but rather qualitative comparisons.

3 Results

3.1 Characterization of base sorbents

The PSD datasets for the as-received metal particles are provided in Figure S1 (Supporting Information) and the average sizes [or $d(0.5)$ values] of the Ag^0, Bi^0, Cu^0, and Sn^0 particles were 18.992, 4.893, 10.276, and 9.810 μm, respectively. The appearances of metal-PAN composite beads before iodine loading are shown in Figure 1. The shapes of beads were ellipsoidal with some irregularities, and the sizes were in the range of 2.29–3.09 mm at the largest diameters (Table S2, Supporting Information). Pure PAN beads without any added metals were white (Figure S2, Supporting Information), but for Ag-PAN, Bi-PAN, Cu-PAN, and Sn-PAN, the composite beads were beige, dark grey, taupe, and light grey, respectively, with some color variabilities from bead to bead that are attributed to fluctuations in metal loadings (Figure 1). These colors matched well with the colors of initial metal particles. All the as-made metal-PAN composite beads were malleable and deformed under pressure with similar degrees of springback. The metal particles in all four separate metal-PAN composites were found to be homogeneously distributed within the different sets of beads. The Ag^0 and Sn^0 particles were relatively larger than Bi^0 and Cu^0 particles within the PAN matrix and could be due to some agglomeration. The densities of the metal-PAN composites (ρ_{pc}) are provided in Table S3 and Figure S3 (Supporting Information) and show somewhat of a linear trend of increasing overall ρ_{pc} with increasing metal densities (ρ_m; see Table S4, Supporting Information) with the exception of Ag-PAN. The Sn-PAN and Ag-PAN densities were the lowest in the series despite the fact that the ρ_m for Ag is the highest and this could be attributed to closed porosity in the Ag-PAN composites not accessible to the He gas.

3.2 Iodine loading data (48 hr)

3.2.1 Appearances

Pictures of the iodine-loaded metal particles and metal-PAN composites are shown in Figure 2a-h and Figure S18 (Supporting Information). The appearances of both metal particles and the metal-PAN composites for each sample set were similar in color where Ag-, Bi-, Cu-, and Sn-based samples were yellow, gray, brown, and orange/brown, respectively, with some slight color shifts between the iodine-loaded metal-PAN composites and the metal particles for Ag and Sn. Figure 2i-p provides SEM micrographs of the metal-PAN composites shown at two different magnifications. The appearances of the metal-iodide complexes varied extensively in size, shape, and morphology between the different samples, and this is attributed to initial metal particle size distributions and shapes (see Figure S1, Supporting Information) as well as the large masses of chemisorbed iodine, which led to swelling of the local composite structure. After iodine loading, the metal-PAN composite surfaces were harder and much less malleable than in the as-made metal-PAN composites. The sizes of the metal-PAN composites did not appear to notably change after iodine loading as shown in Figure S19 (Supporting Information), which might be expected based on the large addition of iodine mass to the composites during loading.

3.2.2 Iodine mass data

The iodine loading capacities of the metal-PAN composite beads and metal particles for 48 h were calculated using the gravimetric methods described in Equations (1), (2), and (3) (see Table 2 as well as Table S6 and Table S7, Supporting Information) and these data are shown graphically in Figure 3a. The results of iodine loading experiments for 48 h at 120±1°C showed Sn-PAN+I with the highest Q_e (m_I/m_s) value of 1.669 followed by Cu-PAN+I with 1.457, Ag-PAN+I with 0.753, and Bi-PAN+I with 0.474 (Figure 3a and Table 2). Pure metal particles showed higher loading capacities over the metal-PAN composites except for Cu^0, and further investigation is required to understand the chemisorption of iodine into PAN composites to explain this particular anomaly (Figure 3 and Table 2).

Based on the precursor masses of metal particles in the metal-PAN composites, the theoretical maximum possible iodine mass uptake was calculated based on formation of the stoichiometric compounds (i.e., Ag → AgI, Bi → BiI_3, Cu → CuI, and Sn → SnI_4) and these were compared to the actual masses of metal particles and metal-PAN composites to achieve the conversion efficiencies on a mass basis [denoted as *C*%m in Equation (10)] shown in Figure 3b and Table 2. For the 48-h exposures, both Ag-PAN and Cu-PAN showed high *C*%m values of 85.4% and 97.2%, respectively, whereas Bi^0 and Sn^0 had *C*%m values of 34.7% and 52.0%, respectively (Figure 3b and Table 2). Nevertheless, the Q_e value of the Sn-PAN composite was higher than Ag-PAN, Bi-PAN, and Cu-PAN due to the formation of SnI_4 (Figure 3a). As for Bi-PAN, the Q_e value was lower than the other metal-PAN composites even with formation of BiI_3 as XRD showed the presence of unreacted Bi^0 phases after iodine loading.

3.2.3 XRD data

The XRD results showed only metal phases of Ag^0, Bi^0, Cu^0, and Sn^0 in the as-made metal-PAN composites and metal particles (see Table 3 and Figure 4). After iodine loading, the metal-iodide phases detected included AgI, BiI_3, CuI, and SnI_4, respectively (see Table 3 and Figure 4 as well as Figures S4, S6, S8, S10, and Table S5, Supporting Information). Based on the XRD refinements, the crystallite sizes of metals in the PAN beads were consistently smaller than crystallite sizes found for the as-received metal particles (Table 3). For Ag-PAN, only the Ag^0 phase was initially present as expected, and during iodine loading at 120±1°C for 48 h, β-AgI (34 mass%) and γ-AgI (66 mass%) phases were formed through chemisorption of $I_{2(g)}$ (Figure 4a and Figure S4, Supporting Information). For Bi-PAN+I, partial conversion of Bi^0 to BiI_3 was observed after 48 h of iodine loading at 120±1°C (Figure 4b). For Cu-PAN+I, only CuI was present after iodine loading for 48 h (Figure 4c). For Sn-PAN+I, Sn^0 particles and $I_{2(g)}$ reacted to form SnI_4, and no other crystalline phases were observed after 48 h (Figure 4d). The formation of the SnI_4 compound was beneficial for the efficiency of iodine capture as one Sn atom captures four iodine atoms. Iodine loading experiments were also performed on pure metal particles that were used for PAN composite synthesis to compare the structural changes during iodine uptake. The results of iodine loading on pure

metal particles showed the same resulting phases as with the metal-PAN composites (see Figures S5, S7, S9, and S11, Supporting Information).

3.3 Time-based study with Bi-based sorbents (24, 48, and 72 h)

To better understand the kinetics of iodine reactions with the Bi-PAN and Bi-Particle sorbents, 24-h and 72-h tests were conducted at 120±1°C. After the 72-h of iodine loading, based on XRD data, all Bi^0 in the Bi-PAN composites and the Bi-Particle materials were fully converted to BiI_3 based on XRD data and the Q_e values were increased to 1.012 (72 h) from 0.474 (48 h) g/g and to 1.382 (72 h) from 0.773 (48 h) g/g, respectively (see Table 2 and Figure 5). Full conversion to iodine-containing compounds for Bi-PAN was slower compared to the other metal-PAN composites, and similar result was observed with Bi^0 particles. Figure 5b shows that, based on mass alone (i.e., expected BiI_3 formation), not all of the Bi^0 was fully reacted to form BiI_3. Figure 5c shows the differences in Q_e values for the Bi-PAN composites and the Bi-Particle samples and the offset between these datasets is attributed to the PAN binder dropping the overall m_m values on a m_s basis.

Figure 6a-c shows the XANES data for the Bi-PAN+I composite sorbents over different iodine exposure times of 24 h, 48 h, and 72 h and Figure 6d shows the extended X-ray absorption fine structure (EXAFS) for iodine-loaded Bi-PAN composites as well as Bi-PAN (without iodine). Figure 6d provides the ability to see the minor fluctuations in the peaks that are associated with the Bi speciation within these samples. Figure 6e provides comparisons of the phase distributions within the different Bi-PAN+I composites in terms of mass fractions of the different components present in the sorbents. It should be noted that the same mass of PAN was added to all metal-PAN composites but the total mass fraction (mf_i of phase "i") of PAN drops in the iodine-loaded metal-PAN composites as the iodine content (and therefore m_{s+I}) increases. The iodine L_3-edge XANES data are shown in Figure S14 (Supporting Information) and do not reveal enough information to discern between the different iodine bonding environments in the Bi-PAN+I composites, BiI_3, and BiOI.

Figure 6f provides a comparison between the BiI_3 concentration based on the mass fraction of BiI_3 (mf_{BiI_3}) in the Bi-PAN+I composites calculated using Equation (15) [mass basis or $mf_{NP,m\text{-}I}$ from Table S10 Supporting Information] and the XANES fitting data [$mf_{BiI_3(XANES)}$; Table S9, Supporting Information], which was converted to a mass basis from the molar concentrations (Table S8, Supporting Information) calculated with Equation (16). Additionally, the iodine L_3-edge XANES data for the Bi-PAN+I composites, BiOI, and BiI_3 look very similar on a qualitative basis (see Figure S14, Supporting Information) suggesting very similar bonding environments for iodine amongst these species.

3.4 Aqueous testing with metal-PAN composites

Iodine capture in the aqueous simulant was not successful. Over the course of the 24 h batch test, the PAN composites were not able to effectively capture iodine-127 (i.e., $^{127}I^-$). It was noticed that the metal-PAN composites changed density during the test, where they initially settled to the bottom of the container, but after 24 h of testing, they rose and floated at the top of the solution. More data is needed to understand why these do not work for iodide capture.

4 Discussion

The method of dropping the DMSO-PAN solutions containing metal particles into water instantly freezes the initial droplet shape into final bead morphology. Allowing the beads to sit in the DIW solution draws out the DMSO from the bead interiors through passive diffusion. To further remove DMSO, the beads were placed in fresh DIW baths to help drive the diffusion process by maintaining the concentration gradient. It is likely that different polymers could be implemented in a similar technique, but PAN was selected based on success of implementing this same process to create other hybrid sorbents.[30,36-42]

When looking at the iodine loadings for all sorbents in this study, none of the sorbents show full reaction (C%m < 100) of the metal to a MI_x compound based solely on a mass gain basis, although several sorbents do show very high C%m values. These data are in contradiction with the XRD results provided in Table 3 and Figure 4 and this is why some of these other calculations were performed such as the residual metal present in the sorbents ($m_{m,r}$) solely based on the mass of metal present in the sorbents (m_m) at the

start of the iodine-loading experiments. When looking at the comparisons of XRD data with the mass basis data (excluding m_{PAN} in the sorbents), the data show some irregularities where XRD showed far less residual metal present and much higher metal-iodide conversions (in all cases; see Table S12, Figure S16, and Figure S17, Supporting Information). The actual cause(s) for the discrepancies is(are) unclear but could be related to non-crystalline metal being present in the iodine-loaded sorbents or crystalline metallic particles being present below XRD detection limits, although these do not seem very plausible due to the high fractions calculated on a mass basis.

The data in Figure 6f align well, but a caveat to these calculations is that the fitting routine used for XANES data showed that some BiOI could be present whereas the calculation to determine $mf_{NP,m\text{-}I}$ purely on a mass uptake basis did not assume the formation of any BiOI and attributes all mass uptake as iodine to form BiI_3. This approach was taken during data analysis because no BiOI was observed in the XRD analyses of the Bi-based sorbents (see Table 3). The residual Bi values present in the samples based on mass data $mf_{NP,m,r}$ (Table S10, Supporting Information) and XANES data $mf_{Bi,r(XANES)}$ (Table S9, Supporting Information) provide evidence that not all of the Bi^0 reacted to form BiI_3 (or other compounds like BiOI). More work is needed to fully elucidate the underlying causes for incomplete metal utilization in these sorbents. Several assumptions were made to achieve the values from these calculations and the main assumption is based on the purities of the starting metal particles where it is possible that they are not as pure as stated by the vendor.

In a previous study where pure metal wires were evaluated as potential sorbents for $I_{2(g)}$, Ag^0, Cu^0, and Sn^0 were identified as promising candidates from several perspectives including the $I_{2(g)}$ affinity as well as the capture kinetics,[34] and this study was a follow up study to that by implementing pure metal particles into semi-porous polymer beads. In addition to these metals, Bi^0 has emerged as a promising $I_{2(g)}$ getter in other recent studies as well,[22,27,31,43,44] so it was included in this study for comparison. More work is needed to understand the correlations (if any) between the initial metal particle sizes and morphologies with the iodine capture potential under different conditions (e.g., iodine centration, temperature, oxidizing conditions). Since each particle used in this study varied in size and morphology (see Figure S1, Supporting

Information), the iodine capture data does not appear to align well with the PSDs of the initial metal particles (see Figure S13, Supporting Information). A caveat to this comparison is that the iodine-to-metal molar ratios (M_I values) in the iodine-loaded materials are very different for each metal so this needs to be considered when comparing the performances of these dissimilar metals. It is also unclear how large of metal particles could be implemented in a hybrid sorbent such as the metal-PAN composite design. A comparison study to evaluate the ideal sizes of metal particles for each specific metal would be a worthwhile follow-up effort and would bridge the current dataset with a previous study on 0.5-mm diameter metal wires.[34]

The iodine loading capacities of PAN composites and metal particles from this study are compared to other chemisorption-based sorbents from previous studies[9,14,22,29-31,34,44-47] in Table S11 (Supporting Information) where the Cu-PAN+I and Sn-PAN+I composites showed notably higher iodine loading capacities compared zeolites. This move from wires to utilizing metals with higher specific surface areas such as small particles, should help increase the interactions with the available metal surfaces in flow-through systems but will likely never be as effective as using microporous and mesoporous substrates with embedded nanosized getters such as the metal-exchanged zeolites, aerogels, or xerogels. However, metal particles embedded in a porous matrix fall in the middle of these different candidate sets of materials where the getter availability is extremely high (i.e., 75 mass% in this study) and the pressure drop should be minimal in a packed bed of these types of bead-based sorbents that are mostly spherical in shape. It is likely that higher metal loadings can be achieved as well based on previous work involving synthesis of PAN-based composite beads.[38]

Upon loading these sorbents with iodine, options exist for embedding them into a cement or grout for disposal (depending on the disposal environment requirements). It is also possible that the polymer binder could be burned off or dissolved away leaving behind a pure metal iodide available for hot pressing into a monolithic waste form with maximum waste loading.

Future work needs to include assessment of sorption kinetics to better understand why Bi^0 behaves so differently from these other metals, requiring far longer times to achieve full conversion of the metal to

the metal-iodide compound, BiI_3. More work is also needed to understand why these metals do not work for capturing I^- in caustic solutions. Being able to selectively pull $^{129}I^-$ out of caustic scrubber solution would be extremely valuable for nuclear cleanup applications.

In some cases, it might be possible (and desired) to recycle the getter metals for creating new sorbents and this would require stripping the iodine off the metals. One option for doing this for Ag-based sorbents is to soak them in Na_2S solution whereby the AgI dissociates, Ag converts to Ag_2S, and the iodine enters solution as I^- where it could be scavenged using an iodide getter.[48] This appears to add unwanted complexity but does provide the option for recycling Ag, which is a precious metal and a hazardous material with disposal restrictions in the U.S. regulated by the Environmental Protection Agency under the Resource Conservation and Recovery Act (RCRA).[49] It is unclear if similar options exist for recycling Bi-based, Cu-based, or Sn-based sorbents, but if these options did exist, it is unlikely that the benefits would outweigh the costs associated with these processes. Loading iodine into high-capacity sorbents such as metal-organic frameworks or conjugated microporous polymers provides more options for capture that also can have recycle options.[50-52] At some point, the final fate of the captured radioiodine needs to be considered and the ideal binding site for iodine is likely as a metal iodide that is chemical stable in a repository environment.

5 Summary and Conclusions

Four sets of metal-PAN composite beads containing 75 mass% of Ag^0, Bi^0, Cu^0, and Sn^0 (25 mass% PAN) were synthesized and tested for iodine loading capacities and these were compared to iodine capture with the initial metal particles (without PAN). The iodine loading capacities were in the range of Q_e = 0.474 to 1.669 g/g with Sn-PAN showing the highest Q_e value (1.669 g/g) followed by Cu-PAN+I (1.457 g/g), Ag-PAN+I (0.753 g/g), and Bi-PAN+I (0.474 g/g) in descending order, after 48-hour loading tests at 120°C. For the 48-hr iodine loading tests, the Ag-PAN composite showed very high Ag utilization (C%m = 85.4%) with lower values for Sn-PAN (C%m = 52.0%) and Bi-PAN (C%m = 34.7%) where all three showed lower iodine capture than the pure metal particles (C%m of 95%, 70%, and 42%, respectively). Interestingly, the Cu-PAN composites performed better (C%m = 97%) than the pure metal particles (C%m = 52%). For the

Bi-PAN composites and Bi-Particles, iodine exposure times of 72 h showed metal utilization values of 74% and 76% (*C*%m), respectively, based on mass changes showing that the kinetics of adsorption are different for Bi^0 than the other metals.

While these materials are very easy to make, scale-up could be challenging due to settling of the metal particles during the synthesis procedure likely leading to a large variation in metal loading distributions from bead to bead in a single batch. Also, the 75 mass% metal loading in these composites was an arbitrary loading selection and this could likely be increased substantially. It is unclear if the pressure drop would be too high if composites such as these were implemented in a packed column, but this should be evaluated in the future. Compared to the iodine loading capacities of zeolites, aerogels, and xerogels, the Sn-PAN and Cu-PAN composite sorbents showed higher Q_e (m_I/m_s) values by approximately 3× compared to aerogels and xerogels, and approximately 5× to 10× compared to zeolites (i.e., Ag-faujasite and Ag-mordenite). Solution-based capture with the metal-PAN composites did not show any iodide capture so more work should be done to evaluate performance of these sorbents at different pH values and ion competition environments.

Data Availability Statement

The original contributions in presented in this study are included in the article, further inquiries can be direct to the corresponding author.

Associated Content

Supporting Information

The Supporting Information is available free of charge at https://pubs.acs.org/.

PSD data, picture of PAN beads, Bi time study comparisons, XANES data, mass basis data, comparisons with literature data.

Author Information

Corresponding Author

Brian J. Riley – Pacific Northwest National Laboratory, Energy and Environment Directorate, Richland, Washington 99352, United States; Tel: 509-372-4651; orcid.org/0000-0002-7745-6730; E-mail: brian.riley@pnnl.gov

Authors

Saehwa Chong – Pacific Northwest National Laboratory, Energy and Environment Directorate, Richland, WA 99354, United States.

R. Matthew Asmussen – Pacific Northwest National Laboratory, Energy and Environment Directorate, Richland, Washington 99352, United States.

Alessandra L. Fujii Yamagata – Pacific Northwest National Laboratory, Energy and Environment Directorate, Richland, Washington 99352, United States.

José Marcial – Pacific Northwest National Laboratory, Energy and Environment Directorate, Richland, Washington 99352, United States.

Sungsik Lee – X-Ray Science Division, Argonne National Laboratory, Lemont, IL 60439, United States.

Carolyn A. Burns – Pacific Northwest National Laboratory, Energy and Environment Directorate, Richland, Washington 99352, United States.

Author Contributions

SC, **BJR**, **RMA**, **ALFY**, **JM**, **SL**, and **CAB** participated in the preparation of the original draft. All authors listed have made a substantial, direct, and intellectual contribution to the work and approved it for publication.

Acknowledgements and Funding

Pacific Northwest National Laboratory (PNNL) is operated by Battelle Memorial Institute for the DOE under contract DE-AC05-76RL01830. Authors thank Dr. Christian Herbert from Dralon for providing the samples of PAN fibers, Troy Garn from Idaho National Laboratory (INL) for helpful discussions

regarding the PAN composite synthesis process, as well as Ken Marsden (INL) and Kim Gray (DOE-NE) for programmatic support. This research used resources of the Advanced Photon Source, a U.S. Department of Energy (DOE) Office of Science user facility operated for the DOE Office of Science by Argonne National Laboratory under Contract No. DE-AC02-06CH11357. The authors are thankful to Mike Perkins for help with some of the graphics in Scheme 1.

References

(1) Jubin, R. T. *A Literature Survey of Methods to Remove Iodine from Off Gas Streams using Solid Sorbents*, ORNL/TM-6607, Oak Ridge National Laboratory, Oak Ridge, TN, 1979.

(2) Danziger, Y.; Pertzelan, A.; Mimouni, M. Transient Congenital Hypothyroidism after Topical Iodine in Pregnancy and Lactation. *Arch. Dis. Child.* **1987**, *62*, 295-296.

(3) Burger, L. L.; Scheele, R. D. *HWVP Iodine Trap Evaluation*, PNNL-14860, Pacific Northwest National Laboratory, Richland, WA, 2004.

(4) Poncin, S.; Gérard, A.-C.; Boucquey, M.; Senou, M.; Calderon, P. B.; Knoops, B.; Lengele, B.; Many, M.-C.; Colin, I. M. Oxidative Stress in the Thyroid Gland: from Harmlessness to Hazard Depending on the Iodine Content. *Endocrinol.* **2007**, *149*, 424-433.

(5) Riley, B. J.; Vienna, J. D.; Strachan, D. M.; McCloy, J. S.; Jerden Jr, J. L. Materials and Processes for the Effective Capture and Immobilization of Radioiodine: A Review. *J. Nucl. Mater.* **2016**, *470*, 307-326.

(6) Bruffey, S. H.; Jubin, R. T.; Jordan, J. A. Capture of Elemental and Organic Iodine from Dilute Gas Streams by Silver-Exchanged Mordenite. *Procedia Chem.* **2016**, *21*, 293-299.

(7) Bruffey, S. H.; Jordan, J. A.; Jubin, R. T.; Parks, M. L.; Watkins, T. R. *Hot Isostatic Pressing of Engineered Forms of I-AgZ*, NTRD-MRWFD-2017-000412, ORNL/SR-2017/707, Oak Ridge National Laboratory, Oak Ridge, TN, 2017.

(8) Matyáš, J.; Ilton, E. S.; Kovařík, L. Silver-Functionalized Silica Aerogel: Towards an Understanding of Aging on Iodine Sorption Performance. *RSC Adv.* **2018**, *8*, 31843-31852.

(9) Riley, B. J.; Kroll, J. O.; Peterson, J. A.; Matyáš, J.; Olszta, M. J.; Li, X.; Vienna, J. D. Silver-Loaded Aluminosilicate Aerogels as Iodine Sorbents. *ACS Appl. Mater. Interfaces* **2017**, *9*, 32907-32919.

(10) Chong, S.; Riley, B. J.; Kuang, W.; Olszta, M. J. Iodine Capture with Mechanically Robust Heat-Treated Ag-Al-Si-O Xerogel Sorbents. *ACS Omega* **2021**, *6*, 11628-11638.

(11) Sava, D. F.; Garino, T. J.; Nenoff, T. M. Iodine Confinement into Metal-Organic Frameworks (MOFs): Low-Temperature Sintering Glasses to form Novel Glass Composite Material (GCM) Alternative Waste Forms. *Ind. Eng. Chem. Res.* **2012**, *51*, 614-620.

(12) Xie, W.; Cui, D.; Zhang, S.-R.; Xu, Y.-H.; Jiang, D.-L. Iodine Capture in Porous Organic Polymers and Metal-Organic Frameworks Materials. *Mater. Horizons* **2019**, *6*, 1571-1595.

(13) Chen, P.; He, X.; Pang, M.; Dong, X.; Zhao, S.; Zhang, W. Iodine Capture Using Zr-Based Metal–Organic Frameworks (Zr-MOFs): Adsorption Performance and Mechanism. *ACS Appl. Mater. Interfaces* **2020**, *12*, 20429-20439.

(14) Zhou, J.; Chen, Q.; Li, T.; Lan, T.; Bai, P.; Liu, F.; Yuan, Z.; Zheng, W.; Yan, W.; Yan, T. Porous Copper-Loaded Zeolites for High-Efficiency Capture of Iodine from Spent Fuel Reprocessing Off-Gas. *Inorg. Chem.* **2022**, *61*, 7746-7753.

(15) Maeck, W. J.; Pence, D. T.; Keller, J. H. *A Highly Efficient Inorganic Adsorber for Airborne Iodine Species (Silver Zeolite Development Studies)*, IN-1224, Idaho Nuclear Corporation - National Reactor Testing Station, Idaho Falls, ID, 1968.

(16) Maeck, W. J.; Pence, D. T. In *11th AEC Air Cleaning Conference, CONF-700816*; Application of the metal zeolites to radioactive air cleaning problems Richland, WA, 1970; Vol. 2.

(17) Pence, D. T.; Duce, F. A.; Maeck, W. J. In *11th AEC Air Cleaning Conference, CONF 700816*; Study of the Adsorption Properties of Metal Zeolites for Airborne Iodine Species Richland, WA, 1970.

(18) Pence, D. T.; Duce, F. A.; Maeck, W. J. In *12th AEC Air Cleaning Conference, CONF 720823*; Developments in the Removal of Airborne Iodine Species with Metal Substituted Zeolites Oak Ridge, TN, 1972.

(19) Thomas, T. R.; Murphy, L. P.; Staples, B. A.; Nichols, J. T. *Airborne Elemental Iodine Loading Capacities of Metal Zeolites and a Method for Recycling Silver Zeolite*, ICP-1119, Idaho National Laboratory, Idaho Falls, ID, 1977.

(20) Sheppard, G. P.; Hriljac, J. A.; Maddrell, E. R.; Hyatt, N. C. In *Mater. Res. Soc.*; Silver Zeolites: Iodide Occlusion and conversion to Sodalite–a potential ^{129} I waste form?; Van Iseghem, P., Ed. 2006; Vol. 932, p 36.31.

(21) Cheng, Q.; Yang, W.; Li, Z.; Zhu, Q.; Chu, T.; He, D.; Fang, C. Adsorption of gaseous radioactive iodine by Ag/13X zeolite at high temperatures. *J. Radioanal. Nucl. Chem.* **2015**, *303*, 1883-1889.

(22) Al-Mamoori, A.; Alsalbokh, M.; Lawson, S.; Rownaghi, A. A.; Rezaei, F. Development of Bismuth-Mordenite Adsorbents for Iodine Capture from Off-Gas Streams. *Chem. Eng. J.* **2020**, *391*, 123583.

(23) Riley, B. J.; Chong, S.; Schmid, J.; Marcial, J.; Nienhuis, E. T.; Bera, M. K.; Lee, S.; Canfield, N. L.; Kim, S.; Derewinski, M. A.; Motkuri, R. K. Role of Zeolite Structural Properties toward Iodine Capture: A Head-to-head Evaluation of Framework Type and Chemical Composition. *ACS Appl. Mater. Interfaces* **2022**, *14*, 18439-18452.

(24) Chong, S.; Riley, B. J.; Peterson, J. A.; Olszta, M. J.; Nelson, Z. J. Gaseous Iodine Sorbents: A Comparison Between Ag-Loaded Aerogel and Xerogel Scaffolds. *ACS Appl. Mater. Interfaces* **2020**, *12*, 26127–26136.

(25) Asmussen, R. M.; Matyáš, J.; Qafoku, N. P.; Kruger, A. A. Silver-Functionalized Silica Aerogels and Their Application in the Removal of Iodine from Aqueous Environments. *J. Haz. Mater.* **2019**, *379*, 119364.

(26) Matyáš, J.; Sannoh, S. E.; Li, X. S. *Development of a Robust Ag^0-Functionalized Silica Aerogel for Capturing Iodine Gas*, PNNL-30732, Pacific Northwest National Laboratory, Richland, WA, 2020.

(27) Matyáš, J.; Ilton, E. S.; Lahiri, N.; Li, X. S.; Silverstein, J. A. *Bismuth-Functionalized Silica Aerogels for Iodine Capture*, PNNL-32086, Pacific Northwest National Laboratory, Richland, WA, 2021.

(28) Riley, B. J.; Chun, J.; Um, W.; Lepry, W. C.; Matyas, J.; Olszta, M. J.; Li, X.; Polychronopoulou, K.; Kanatzidis, M. G. Chalcogen-Based Aerogels As Sorbents for Radionuclide Remediation. *Environ. Sci. Technol.* **2013**, *47*, 7540-7547.

(29) Subrahmanyam, K. S.; Sarma, D.; Malliakas, C. D.; Polychronopoulou, K.; Riley, B. J.; Pierce, D. A.; Chun, J.; Kanatzidis, M. G. Chalcogenide Aerogels as Sorbents for Radioactive Iodine. *Chem. Mater.* **2015**, *27*, 2619-2626.

(30) Riley, B. J.; Pierce, D., A; Chun, J.; Matyáš, J.; Lepry, W. C.; Garn, T.; Law, J.; Kanatzidis, M. G. Polyacrylonitrile-Chalcogel Hybrid Sorbents for Radioiodine Capture. *Environ. Sci. Technol.* **2014**, *48*, 5832-5839.

(31) Tian, Z.; Chee, T.-S.; Zhu, L.; Duan, T.; Zhang, X.; Lei, L.; Xiao, C. Comprehensive Comparison of Bismuth and Silver Functionalized Nickel Foam Composites in Capturing Radioactive Gaseous Iodine. *J. Haz. Mater.* **2021**, *417*, 125978.

(32) *CRC Handbook of Chemistry and Physics*; 88th ed.; CRC Press: Boca Raton, FL, 2007-2008.

(33) Gattu, V. K.; Stariha, S.; Lee, E.; Fortner, J. A.; Ebert, W. L. *Degradation Tests with Iodide Waste Forms: FY20 Status Report*, ANL/CFCT-20/22, Argonne National Laboratory, Lemont, IL, 2020.

(34) Riley, B. J.; Chong, S.; Beck, C. L. Iodine Vapor Reactions with Pure Metal Wires at Temperatures of 100-139 °C in Air. *Ind. Eng. Chem. Res.* **2021**, *60*, 17162-17173.

(35) Holladay, D. W. *A Literature Survey: Methods for the Removal of Iodine Species from Off-Gases and Liquid Waste Streams of Nuclear Power and Nuclear Fuel Reprocessing Plants, with Emphasis on Solid Sorbents*, ORNL/TM-6350, Oak Ridge National Laboratory, Oak Ridge, TN, 1979.

(36) Cordova, E. A.; Garayburu-Caruso, V.; Pearce, C. I.; Cantrell, K. J.; Morad, J. W.; Gillispie, E. C.; Riley, B. J.; Colon, F. C.; Levitskaia, T. G.; Saslow, S. A. Hybrid Sorbents for ^{129}I Capture from Contaminated Groundwater. *ACS Appl. Mater. Interfaces* **2020**, *12*, 26113-26126.

(37) Riley, B. J.; Chong, S.; Asmussen, R. M.; Bourchy, A.; Engelhard, M. H. Polyacrylonitrile Composites of Ag-Al-Si-O Aerogels and Xerogels as Iodine and Iodide Sorbents. *ACS Appl. Polymer Mater.* **2021**, *3*, 3344-3353.

(38) Riley, B. J.; Chong, S.; Kuang, W.; Varga, T.; Helal, A. S.; Galanek, M.; Li, J.; Nelson, Z. J.; Thallapally, P. K. Metal-Organic Framework-Polyacrylonitrile Composite Beads for Xenon Capture. *ACS Appl. Mater. Interfaces* **2020**, *12*, 45342-45350.

(39) Riley, B. J.; Garn, T. *Purification of Gas and Liquid Streams Using Composite Sorbents Embedded in a Polyacrylonitrile Matrix*; Nova Science Publishers, 2019; Vol. 35.

(40) Garn, T. G.; Greenhalgh, M.; Law, J. D. Development and Evaluation of a Silver Mordenite Composite Sorbent for the Partitioning of Xenon from Krypton in Gas Compositions. *J. Nucl. Sci. Technol.* **2015**, *53*, 1484-1488.

(41) Greenhalgh, M.; Garn, T. G.; Law, J. D. Development of a hydrogen mordenite sorbent for the capture of krypton from used nuclear fuel reprocessing off-gas streams. *J. Nucl. Sci.Tech.* **2014**, *51*, 476-481.

(42) Welty, A. K.; Greenhalgh, M.; Garn, T. G. *Preliminary Desorption Studies for HZ-PAN and AgZ-PAN*, NTRD-MRWRD-2017-000207, INL/EXT-17-43231, Idaho National Laboratory, Idaho Falls, ID, 2017.

(43) Reda, A. T.; Pan, M.; Zhang, D.; Xu, X. Bismuth-Based Materials for Iodine Capture and Storage: A Review. *J. Environ. Chem. Eng.* **2021**, *9*, 105279.

(44) Yang, J. H.; Shin, J. M.; Park, J. J.; Park, G. I.; Yim, M. S. Novel Synthesis of Bismuth-Based Adsorbents for the Removal of ^{129}I in Off-Gas. *J. Nucl. Mater* **2015**, *457*, 1-8.

(45) Riley, B. J.; Chong, S.; Marcial, J.; Lahiri, N.; Bera, M. K.; Lee, S.; Wu, T.; Kruska, K.; Matyáš, J. Silver-loaded xerogel nanostructures for iodine capture: A comparison of thiolated versus unthiolated sorbents. *ACS Appl. Nano Mater.* **2022**.

(46) Strachan, D. M.; Chun, J.; Matyas, J.; Lepry, W.; Riley, B. J.; Ryan, J. V.; Thallapally, P. K. *Summary Report on the Volatile Radionuclide and Immobilization Research for FY2011 at PNNL*, FCRD-SWF-2011-000378, PNNL-20807, Pacific Northwest National Laboratory, Richland, WA, 2011.

(47) Riley, B. J.; Chong, S.; Olszta, M. J.; Peterson, J. A. Evaluation of Getter Metals in Na-Al-Si-O Aerogels and Xerogels for the Capture of Iodine Gas. *ACS Appl. Mater. Interfaces* **2020**, *12*, 19682-19692.

(48) Cao, C.; Chong, S.; Thirion, L.; Mauro, J. C.; McCloy, J. S.; Goel, A. Wet Chemical Synthesis of Apatite-Based Waste Forms – A Novel Room Temperature Method for the Immobilization of Radioactive Iodine. *J. Mater. Chem. A* **2017**, *5*, 14331-14342.

(49) Environmental Protection Agency: Washington, D.C., 2012; Vol. 40 CFR 261.

(50) Liao, Y.; Weber, J.; Mills, B. M.; Ren, Z.; Faul, C. F. J. Highly Efficient and Reversible Iodine Capture in Hexaphenylbenzene-Based Conjugated Microporous Polymers. *Macromol.* **2016**, *49*, 6322-6333.

(51) Yu, Q.; Jiang, X.; Cheng, Z.; Liao, Y.; Duan, M. Porous ZIF-8@Polyacrylonitrile Composite Beads for Iodine Capture. *RSC Adv.* **2021**, *11*, 30259-30269.

(52) Lee, Y. R.; Do, X. H.; Cho, K. Y.; Jeong, K.; Baek, K.-Y. Amine-Functionalized Zeolitic Imidazolate Framework-8 (ZIF-8) Nanocrystals for Adsorption of Radioactive Iodine. **2020**, *3*, 9852-9861.

Tables

Table 1. Details from batching metal-PAN composites including the total mass of PAN, volume of DMSO used, and mass of metal particles added.

Sample	PAN (g)	DMSO (mL)	Metal (g)
Ag-PAN	0.2014	3.0	0.6015
Bi-PAN	0.2008	3.0	0.6012
Cu-PAN	0.2002	3.0	0.6010
Sn-PAN	0.2002	3.0	0.5994

Table 2. Iodine loading measured with a gravimetric method listing experimental time (t, hr) samples were exposed to 120±1°C, sample mass (m_s), iodine-loaded sample masses (m_{s+I}), iodine mass (m_I), m_I/m_s, iodine mass uptake ($m\%_I$), maximum iodine mass possible ($m_{I,max}$) based on full metal-iodine chemisorption) to form MI_x, the maximum possible iodine mass uptake based on target metal-iodide stoichiometries ($Q_{e,max}$), and the actual conversion % based on mass data ($C\%m$). Iodine exposure times were 48 h unless otherwise labeled in sample IDs.

Sample ID	t (hr)	m_s (g)	m_{s+I} (g)	m_I (g)	$m\%_I$ (mass%)	m_I/m_s (g g^{-1})	$m_{I,max}$ (g)	$Q_{e,max}$ (g/g)	$C\%m$ (mass%)
Ag-PAN+I	48	0.0369	0.0647	0.0278	42.97	0.753	0.0326	0.882	85.4%
Bi-PAN+I	48	0.0293	0.0432	0.0139	32.18	0.474	0.0400	1.366	34.7%
Cu-PAN+I	48	0.0276	0.0678	0.0402	59.29	1.457	0.0413	1.498	97.2%
Sn-PAN+I	48	0.0359	0.0958	0.0599	62.53	1.669	0.1151	3.207	52.0%
Ag-Particle+I	48	0.0292	0.0619	0.0327	52.83	1.120	0.0344	1.176	95.2%
Bi-Particle+I	48	0.0216	0.0383	0.0167	43.60	0.773	0.0394	1.822	42.4%
Cu-Particle+I	48	0.0214	0.0435	0.0221	50.80	1.033	0.0427	1.997	51.7%
Sn-Particle+I	48	0.0275	0.1100	0.0825	75.00	3.000	0.1176	4.276	70.2%
Bi-PAN+I(24h)	24	0.0196	0.0268	0.0072	26.87	0.367	0.0268	1.366	26.9%
Bi-PAN+I(72h)	72	0.0331	0.0666	0.0335	50.30	1.012	0.0452	1.366	74.1%
Bi-Particle+I(24h)	24	0.0147	0.0230	0.0083	36.09	0.565	0.0268	1.822	31.0%
Bi-Particle+I(72h)	72	0.0246	0.0586	0.0340	58.02	1.382	0.0448	1.822	75.9%

Table 3. XRD data including phases, phase concentrations (mass%), and crystallite size (nm) for the metal-PAN composites and metal particles after iodine loading based on Rietveld refinements.

Sample	Phases	Concentration (mass%)	Crystallite size (nm)
Ag-PAN	Ag^0	100	79
Bi-PAN	Bi^0	100	232
Cu-PAN	Cu^0	100	87
Sn-PAN	Sn^0	100	101
Ag-Particle	Ag^0	100	116
Bi-Particle	Bi^0	100	277
Cu-Particle	Cu^0	100	109
Sn-Particle	Sn^0	100	186
Ag-PAN+I	β-AgI, γ-AgI	34.15, 65.85	57, 66
Bi-PAN+I	Bi^0, BiI_3	15.47, 84.53	165, 68
Cu-PAN+I	CuI	100	77
Sn-PAN+I	SnI_4	100	255
Ag-Particle+I	β-AgI, γ-AgI	21.63, 78.37	108, 98
Bi-Particle+I	Bi^0, BiI_3	14.65, 85.35	232, 68
Cu-Particle+I	CuI	100	97
Sn-Particle +I	SnI_4	100	159
Bi-PAN+I-24h	Bi^0, BiI_3	27.51, 72.49	156, 49
Bi-PAN+I-72h	BiI_3	100	77
Bi-Particle+I-24h	Bi^0, BiI_3	23.47, 76.53	221, 62
Bi-Particle+I-72h	BiI_3	100	106

Schemes

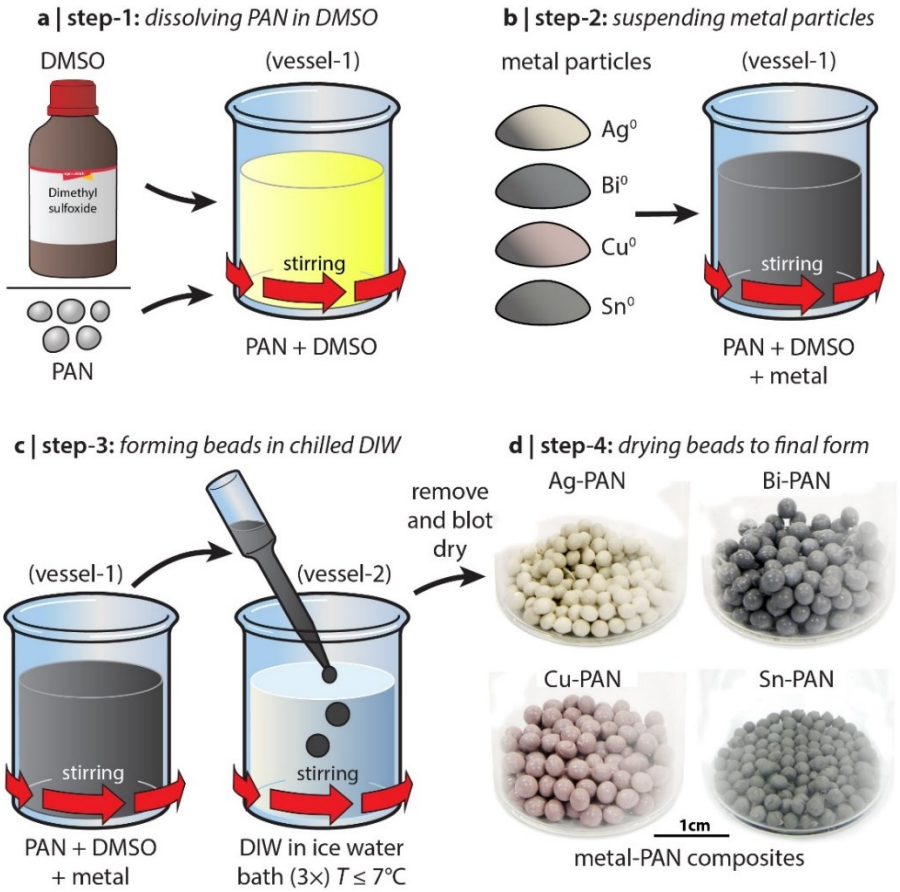

Scheme 1. Process flow diagram showing how the metal-PAN composites are synthesized including (a, step-1) dissolving PAN into DMSO, (b, step-2) suspending metal particles in the DMSO-PAN mixture, (c, step-3) forming beads by dropping the DMSO-PAN-metal mixture in water, and (d, step-4) the final dried metal-PAN composite beads.

Figures

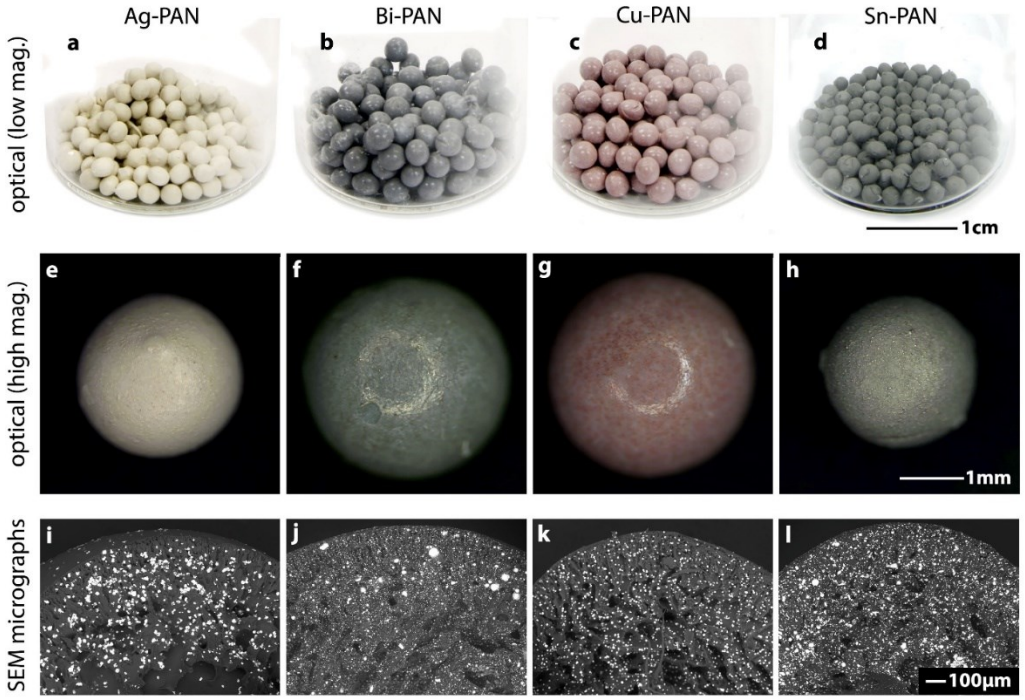

Figure 1. (a-h) Optical images of full composite beads of (a,e) Ag-PAN, (b,f) Bi-PAN, (c,g) Cu-PAN, and (d,h) Sn-PAN. (i-l) SEM micrographs of internal surfaces of as-made metal-PAN composites (micrographs taken at the perimeter of each bead).

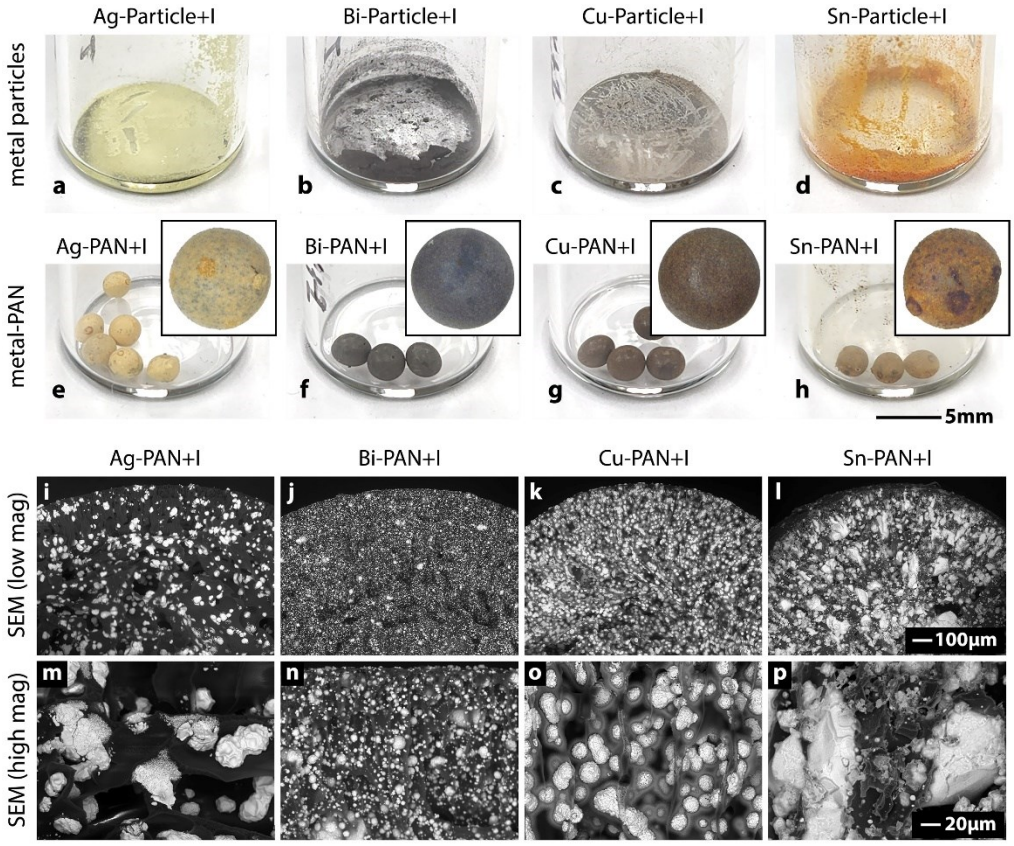

Figure 2. (a-h) Pictures of iodine-loaded samples including (a-d) metal particles and (e-h) metal-PAN composites including those with (a,e) Ag, (b,f) Bi, (c,g) Cu, and (d,h) Sn. (e-h) Image insets show higher-resolution images of a single metal-PAN composite for each sample. (i-p) SEM micrographs of metal-PAN composites loaded with iodine for 48 hours taken at two different magnifications including (a,e) Ag-PAN+I, (b,f) Bi-PAN+I, (c,g) Cu-PAN+I, and (d,h) Sn-PAN+I.

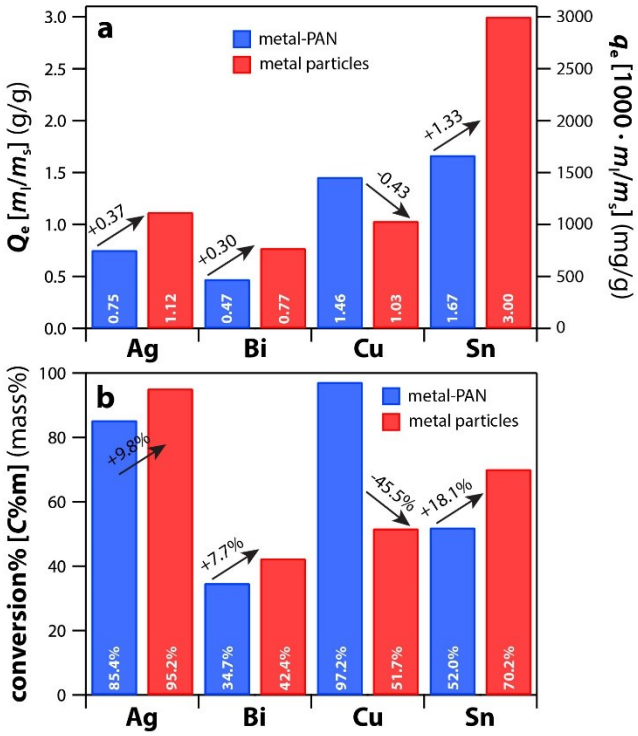

Figure 3. Summary of (a) Q_e (m_I/m_s) and q_e ($1000 \cdot m_I/m_s$) data [see Equation (3) and Equation (4)] and (b) conversion% [i.e., *C*%m; see Equation (10)] for both metal-PAN composites and the metal particles for the 48-hour experiments. For (a), the maximum possible ($Q_{e,max}$) iodine loadings ($m_{I,max}/m_s$) are provided in Table 2.

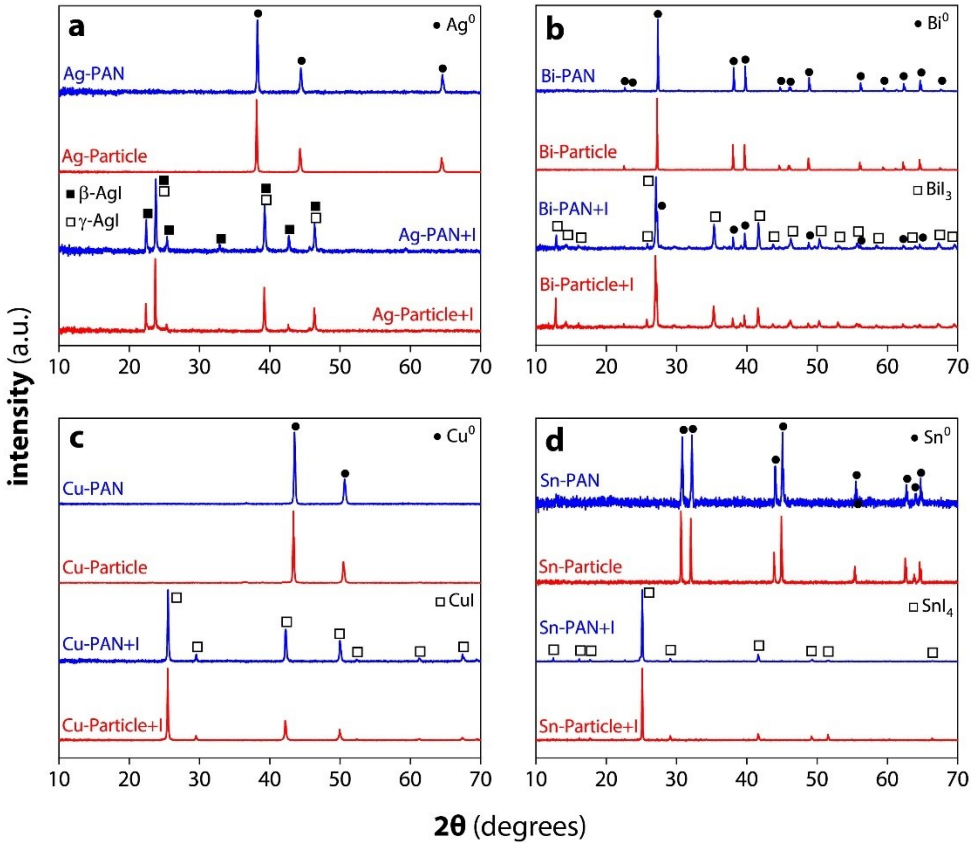

Figure 4. XRD patterns and phases of (a) Ag, (b) Bi, (c) Cu, and (d) Sn metal-PAN composites and metal particles before and after iodine loading at 120±1 °C for 48 hours.

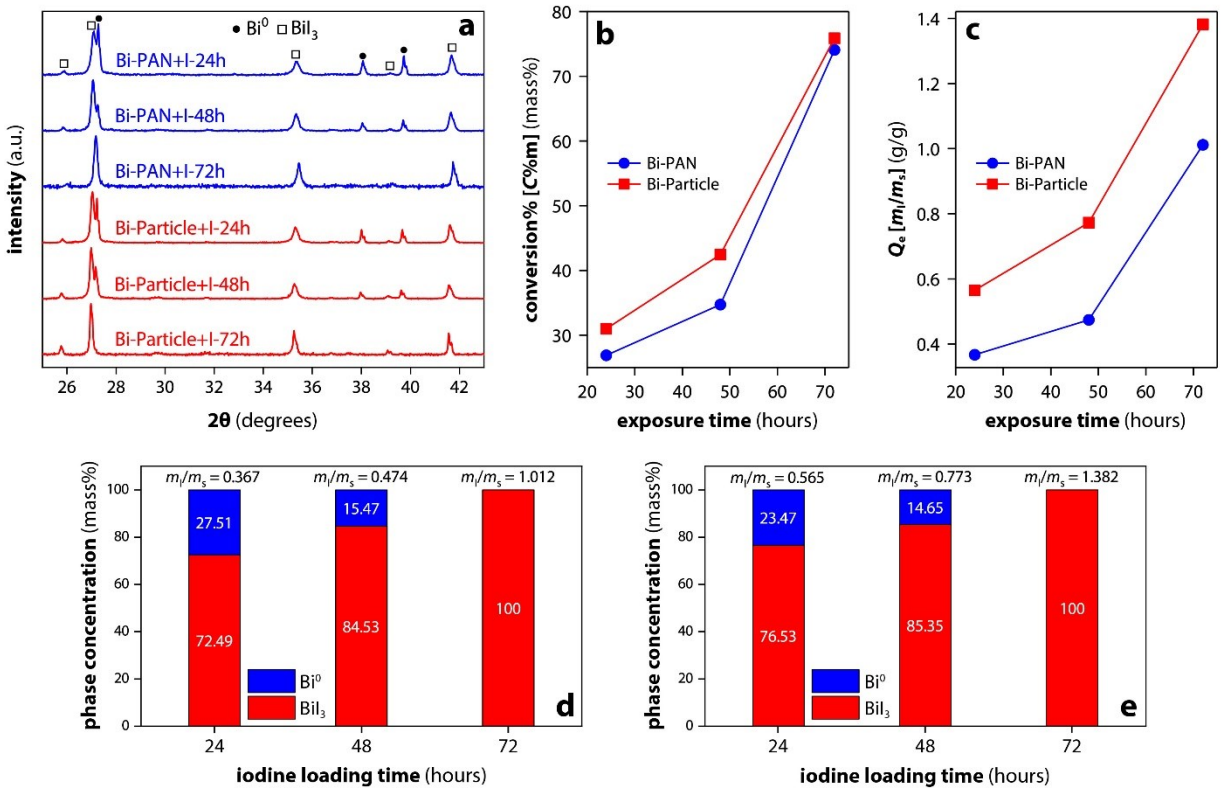

Figure 5. Data for Bi-PAN and Bi-Particles over time (t = 24, 48, and 72 hours). (a) XRD patterns showing conversion of Bi^0 to BiI_3 phases, (b) phase conversion% (C%m) based on iodine mass data [see Equation (10), (c) Q_e (m_l/m_s) data [see Equation (3)], (d) XRD phase distribution for Bi-PAN composites, and (e) XRD phase distribution for Bi-Particles.

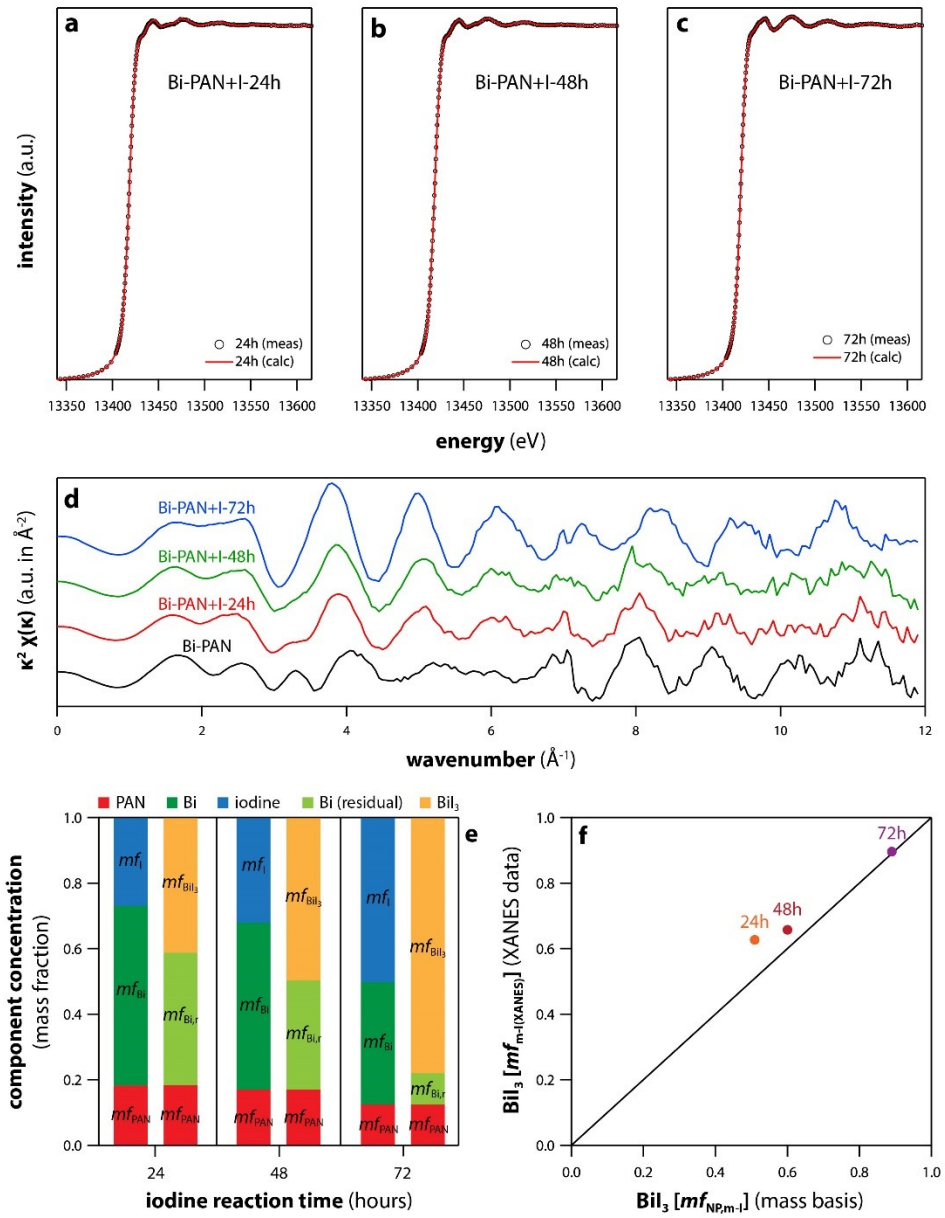

Figure 6. Data comparisons for Bi-PAN composites loaded with iodine. (a-d) XAS data including measured and calculated datasets for (a-c) XANES at (a) 24 h, (b) 48 h, and (c) 72 h of iodine exposure time as well as (d) showing the fluctuations in the intensities between samples in the EXAFS region. (e) Mass fractions of components in the Bi-PAN+I including showing mf_{PAN}, mf_{Bi}, mf_{I}, $mf_{Bi,r}$, and mf_{BiI_3} in the iodine-loaded samples, respectively. (f) Comparison between the BiI_3 mass fractions in the 24-h, 48-h, and 72-h samples calculated by mass changes [i.e., $mf_{NP,m\text{-}I}$; see Table S10, Supporting Information) and XANES fitting [i.e., $mf_{BiI_3(XANES)}$; see Table S9, Supporting Information].

TOC graphic

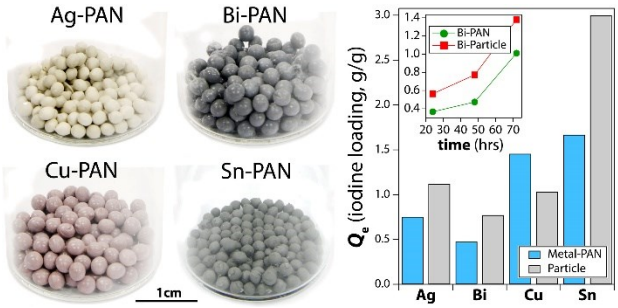
Ag-PAN
Bi-PAN
Cu-PAN
Sn-PAN
1cm
Bi-PAN
Bi-Particle
time (hrs)
Q_e (iodine loading, g/g)
Metal-PAN
Particle
Ag
Bi
Cu
Sn